THESIS FOR THE DEGREE OF LICENTIATE OF ENGINEERING

Interactions Between Localized Surface Plasmons and Molecular Resonances

GÜLIS ZENGIN

Department of Applied Physics

CHALMERS UNIVERSITY OF TECHNOLOGY

Göteborg, Sweden 2013

Interactions Between Localized Surface Plasmons and Molecular Resonances
GÜLIS ZENGIN

Department of Applied Physics
Chalmers University of Technology
SE-412 96 Göteborg
Sweden
Telephone + 46 (0) 31 772 3228

Cover:
Schematic diagram of spherical silver nanoparticle coated with thiolated Rhodamine 6G. See further, Paper I, Figure 1

Chalmers reproservice
Göteborg, Sweden, 2013

Interactions Between
Localized Surface Plasmons and Molecular Resonances

Gülis Zengin
Department of Applied Physics
Chalmers University of Technology

Abstract

Molecular plasmonics is the study of interactions between plasmonic nanostructures and molecules. It has been basis for fundamental understanding of light-matter interactions and development of many technological applications, such as biological and chemical sensing, plasmon-enhanced spectroscopies, optical switches, and plasmon-enhanced energy harvesting. When the plasmon energy of a metal nanostructure is degenerate with the absorption energy of a nearby molecule, the interaction becomes resonant. Strong and confined electromagnetic field induced by the metal nanoparticle polarizes the molecule. This consecutively modifies the electron oscillations in the metal nanostructures. As a result, optical responses of both the molecules and the plasmonic nanostructures are changed by the interaction of the molecule and plasmons.

Organic chromophores interacting with plasmonic nanostructures constitutes an important part in the molecular plasmonics field. Rhodamine 6G is one of the organic chromophores that has been widely studied with the interaction of silver nanostructures in the context of single molecule surface-enhanced Raman spectroscopy. In this thesis, spectral dips in the Rayleigh scattering of single silver nanoparticles interacting with Rhodamine 6G have been shown for the first time. This was achieved by using a novel way of adsorbing Rhodamine 6G on silver surface. Similar observations have been reported between single plasmonic nanoparticles and chromophores. However, the mechanism behind was only explained by strong coupling or plasmon resonant energy transfer. Mie theory calculations suggest that surface-enhanced absorption significantly contributes to these spectral modifications as well as the coupling. The strength of molecule-plasmon interactions is strongly affected by the properties of plasmonic nanoparticles and chromophores. By decreasing the radiative damping of plasmonic particles, and using J-aggregates of a cyanine dye, which exhibit high oscillator strength and narrow transition linewidth, it is possible to approach strong coupling regime. In this thesis we observed 50% transparency in the scattering spectra of single silver nanorods. To our knowledge, this is the strongest modification reported up to date at single particle level.

Keywords: Localized surface plasmon resonance, Rhodamine 6G,
J-aggregates, single particles, surface-enhanced absorption, strong coupling

Appended Papers

The following papers are included in this licentiate thesis:

Paper 1: ***Interaction between Localized Surface Plasmons and Thiolated Rhodamine 6G***
Gülis Zengin, Tina Gschneidtner, Tomasz J. Antosiewicz, Kasper Moth-Poulsen, Timur Shegai, and Mikael Käll
In manuscript.
My contribution: *I prepared some of the samples, conducted most of the optical experiments and all SEM measurements. I analysed the data. I wrote a draft of the paper.*

Paper 2: ***Approaching the strong coupling limit in single plasmonic nanoparticles interacting with J-aggregates***
Gülis Zengin, Göran Johansson, Peter Johansson, Mikael Käll, and Timur Shegai
Submitted manuscript.
My contribution: I participated in discussions, and in the design of the experiments. I conducted SEM measurements, and wrote a part of the paper.

This paper is not included in the thesis:
A bimetallic nanoantenna for directional colour routing
Nature Communications, 2, 481 (2011).
Timur Shegai, Si Chen, Vladimir D. Miljkovic, Gülis Zengin, Peter Johansson, Mikael Käll

Contents

Chapter 1

Introduction

Plasmonics is an emerging area of nanophotonics. It is the study of light interacting with metal nanostructures that can support surface plasmon excitations. This effect is based on coherent oscillations of the surface conduction electrons excited by electromagnetic radiation. Plasmonic metal nanostructures provide the ability to control and manipulate light at nanometre scale [1–4].

The study of plasmonics triggered the development of innovative optical materials and yielded insightful theoretical understanding. This resulted in novel applications and devices spanning a wide range of disciplines, ranging from life sciences to energy harvesting [3]. Since the interaction between surface plasmons and nearby molecules constitutes the basics of most of these applications, the study of molecule-plasmon interaction, known as molecular plasmonics, became a significant sub-field of plasmonics. This field of study has led to a better understanding and control of the interaction between surface plasmons and molecules. This has been proven to be useful for the purposes of the design of pioneering materials, devices, and tools, which could be utilized in a wide variety of research disciplines [5–7].

Precise spatial and spectral control of plasmonic nanostructures as well as the positioning of molecules near metal surfaces are crucial for effective molecule-plasmon interactions. It requires advanced nanofabrication, chemical synthesis, surface and molecular functionalization, molecular self-assembly, and accurate measurements, and computational tools to model, design, control, and characterize molecules on metal surfaces. Therefore with these improvements there has been progress in the field of molecular plasmonics. For instance developments in chemical synthesis has made it possible to synthesize highly crystalline nanoparticles of different shapes, sizes and compositions by forming particles on an atom-by-atom basis [8]. Improvements in lithography techniques enabled fabrication of nanoparticles that are controlled in size, shape, and position on a substrate. This method is key for controlling the spacing of plasmonic particles which then leads to particle-particle interactions. Moreover, novel methods were developed by combining chemical and lithographic techniques such as colloidal lithography which render possible the fabrication of plasmonic structures at nanometre scale over large areas [9]. Even though it is still a challenge to precisely, specifically, and selectively position molecules in a certain configuration and orientation on metal nanostructures in a robust way, different surface functionalization techniques have been developed by using chemical bonds, electrostatic interactions or biological recognitions. Molecular

self-assembly has become a powerful way to immobilize molecules on metal surfaces [8]. Advances in optical imaging and spectroscopy techniques, such as dark-field microscopy, facilitate the measurement of plasmon-molecule nanocomplexes on a single particle level. This provides detailed information about the properties of nanostructures that are not measurable on ensemble level [3]. These improvements in both plasmonics and molecular nanotechnology have progressively shifted the focus of molecular plasmonics from developing plasmonic molecule complexes and investigating their physical properties to the potential applications of these complexes. The broad spectrum of applications includes biological and chemical sensors [10], surface-enhanced spectroscopies [11,12] , plasmon resonance energy transfer (PRET) [13,14], plasmon enhanced solar light harvesting [15], near-field scanning optical microscopy [16], single molecule detectors [17], targeted delivery [18], optical tweezers [19], and optical switches of gene interference [20]. In florescence-based applications, interactions of metal nanostructures with fluorophores can have many useful effects, including increased quantum yields, increased photostability, increased distances for resonance energy transfer, and decreased lifetimes. These changes can result in improved sensitivity and photostability, and decreased interference from unwanted background emission [21].

Molecules can interact with plasmonic nanostructures optically, thermally or mechanically [8]. In this thesis I will focus on the former mode of interaction. Localized surface plasmon resonance (LSPR) based sensing [22], d fluorescence (SEF) [23], surface-enhanced Raman spectroscopy (SERS) [24], molecule-plasmon hybridization [25], and plasmon energy transfer (PRET) [26] are examples of optical interaction. Optical interaction between molecules and collective excitation of conduction electrons in metal nanoparticles substantially depends on the electronic structure of molecules. If the molecule has resonant absorbance overlapping with surface plasmons, we can observe plasmon resonant energy transfer or plasmon hybridization. Chapter Two describes both non-resonant and resonant coupling between plasmonic nanostructures and molecules, with examples from my own research and literature. Chapter Three provides sample preparation, surface functionalization, as well as optical characterization methods. Chapter Four gives a summary and future outlook of the research field.

Chapter 2

Background

Plasmon-molecule interactions highly depend on the electronic structure of the molecule and can be categorized into two kinds of interactions, non-resonant coupling and resonant coupling. Non-resonant coupling takes place when the excitation energy of the molecule is not overlapping with the plasmon resonance energy. On the contrary resonant coupling occurs in case of a spectral overlap between molecular absorption and plasmon resonance [7]. This chapter will provide the basics of different molecule-plasmon interactions and some examples from my own research.

2.1. Non-resonant coupling

For non-resonant interactions molecules either do not show molecular extinction or molecular the extinction energy is spectrally far away from the plasmon resonance energy [6]. These molecules can be considered as being a non-absorbing dielectric medium for the plasmonic nanostructures. Two types of non-resonant coupling are described in this section, refractive index dependent plasmon shift and non-resonant surface-enhanced Raman scattering (SERS).

2.1.1. Refractive index dependent plasmon resonance

Plasmon oscillations can be described by classical physics, where the collective oscillations of free electrons in metals are modelled as a damped harmonic oscillator (the Lorentz model). An external electric field gives rise to displacement of the electron gas with reference to the ionic cores [27]. This induces a restoring electric field inside and outside of the particle. If there is a non-absorbing molecule or solvent with high dielectric function, these restoring forces become weaker by shifting the plasmon resonance to lower energies (redshift in wavelength) [7]. The relation between the polarizability of a spherical metal nanoparticle and the dielectric function of the surrounding medium (alternatively, refractive index) can be understood from the following formula based on the quasi-static approximation. The complex polarizability defining the induced dipole moment inside the particle induced by the external field is given as [28]:

$$\alpha(\omega) = 4\pi a^3 \frac{\varepsilon_{metal}(\omega) - \varepsilon_{medium}}{\varepsilon_{metal}(\omega) + 2\varepsilon_{medium}} \qquad (2.1)$$

In this relation, a is the radius of the spherical particle. The dielectric function of the metal can be approximated by the free electron Drude model with ω_p as the plasma frequency and γ as the damping factor:

$$\varepsilon_{metal}(\omega) = 1 - \frac{\omega_p^2}{\omega^2 + i\omega\gamma} \tag{2.2}$$

The polarizability undergoes a resonant condition when $Re[\varepsilon_{metal}(\omega) = -2\varepsilon_{medium}]$ and $Im[\varepsilon_{metal}(\omega)]$ is small or slowly varying. By using the complex polarizability scattering, absorption, and extinction cross sections can be calculated via the Poynting vector, where $\varepsilon_{metal} = \varepsilon_1 + i\varepsilon_2$ [29].

$$C_{sca} = \frac{k^4}{6\pi}|\alpha|^2 = \frac{8\pi}{3}k^4a^6\left|\frac{\varepsilon_{metal}(\omega) - \varepsilon_{medium}}{\varepsilon_{metal}(\omega) + 2\varepsilon_{medium}}\right|^2 \tag{2.3}$$

$$C_{abs} = kIm[\alpha] = 4\pi ka^3 Im\left[\frac{\varepsilon_{metal}(\omega) - \varepsilon_{medium}}{\varepsilon_{metal}(\omega) + 2\varepsilon_{medium}}\right] \tag{2.4}$$

$$C_{ext} = C_{sca} + C_{abs} \tag{2.5}$$

$$C_{ext} = 9\frac{\omega}{c}\varepsilon_{medium}^{3/2}V\frac{\varepsilon_2}{|\varepsilon_1 + 2\varepsilon_{medium}|^2 + {\varepsilon_2}^2} \tag{2.6}$$

By measuring the shift in the plasmon peak position in the extinction spectrum, it is possible to sense different molecules and solvents by refractive index change. Shift in the peak position can be extracted by fitting the plasmon resonance peak to a Lorentzian function. In Figure 2.1 the consecutive adsorption of different molecules on the same gold nanodisks is shown. The plasmon peak position shift depends on both the molecule and the buffer solution. The gold nanodisks were prepared by hole-mask colloidal lithography, and they are 100 nm in diameter and 30 nm in height. They show a plasmon peak position at around 658 nm in the first buffer. The first injected solution is mixture of thiolated polyethyleneglycol (PEG) and thiolated polyethyleneglycol biotin (PEG-bio). Thiol covalently binds to the gold surface, which results in a red shift in peak position of 8 nm. As buffer 1 is exchanged with buffer 2, that has a lower salt concentration, the plasmon peak position blue shifts 4 nm. The injection of polylysine-graft-polyethyleneglycol (PLL-g-PEG) does not result in a large shift in the plasmon peak position because it mainly binds to the glass substrate. Finally, streptavidin coated quantum dots (SA-QD) are introduced, and they bind to the biotin-adsorbed surface, giving rise to around 2.5 nm peak shift.

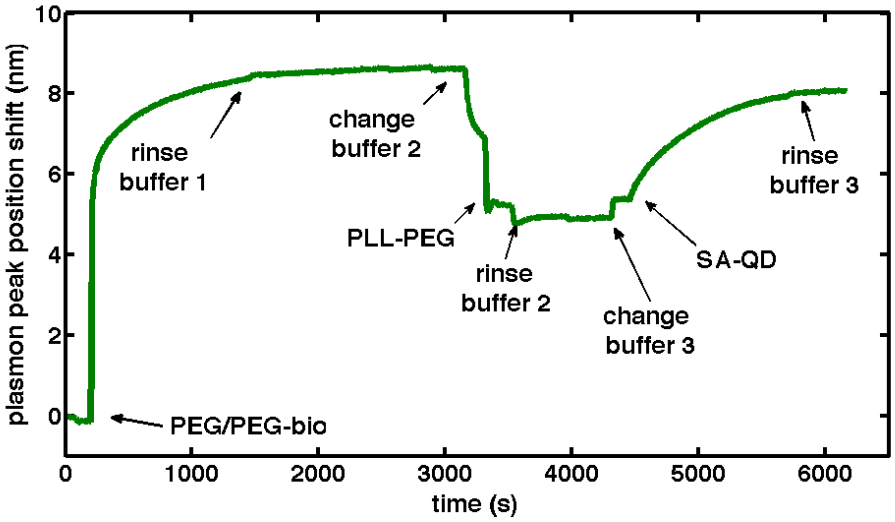

Figure 2.1. Change in the plasmon peak position by adsorption of different polymers and proteins (PEG/PEG-bio, PLL-g-PEG, SA-QD) on gold nanoparticles in different buffer solutions.

2.1.2 Non-resonant surface-enhanced Raman scattering

Electromagnetic enhancement of SERS

When a molecule is placed close to a metal nanoparticle, the excitation of the surface plasmon greatly increases the local field experienced by the molecule. The nanoparticle does not only enhance the incident field but also the Raman scattering from the molecule [7].

In the absence of plasmonic nanoparticles, the total Stokes Raman signal from a molecule $P^{RS}(\omega_s)$ is proportional to the Raman cross section of the molecule σ_{free}^{R}, the excitation laser intensity $I(\omega_s)$, and the number of molecules in the probed volume N [30].

$$P^{RS}(\omega_s) = N\sigma_{free}^{R} I(\omega_s) \tag{2.7}$$

When the molecule is in the vicinity of the metal nanoparticle, experimental observations suggest that the total Stokes Raman signal $P^{SERS}(\omega_s)$ is modified by two effects, the enhancement of local electromagnetic fields, and a chemical enhancement. We express the electromagnetic enhancement factors for the laser and the Raman scattered field as $A(\omega_L)$ and $A(\omega_s)$ respectively (ω_L is the laser frequency and ω_s is the frequency of the Raman scatted field). With the chemical enhancement the molecule experiences a different Raman process, described by a new Raman cross-section σ_{ads}^{R}. The number of molecules involved in the SERS process is N'. The total SERS signal can be written as

$$P^{SERS}(\omega_s) = N'\sigma_{ads}^{R}|A(\omega_L)|^2|A(\omega_s)|^2 I(\omega_L) \tag{2.8}$$

If we consider a small metal sphere in the quasi-static approximation (see Section 2.1), the distribution of the induced electric field E_{sp} of a point dipole in the centre of the metal sphere is given by the following formula. Note that this formula is given for the molecules oriented in the dipole orientation of the metal sphere.

$$E_{sp} = \frac{\varepsilon_{metal}(\omega) - \varepsilon_{medium}}{\varepsilon_{metal}(\omega) + 2\varepsilon_{medium}} \frac{r^3}{(r+d)^3} E_0 \tag{2.9}$$

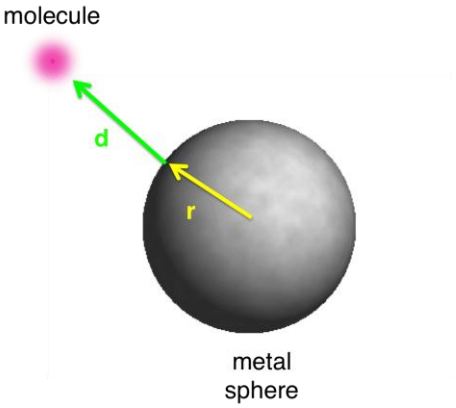

Figure 2.2. Schematic diagram for illustration of the concept of electromagnetic SERS enhancement

If the molecule is at a distance d from the surface of the metal sphere, as drawn in Figure 2.2, it experiences the field $E_{molecule}$, which is the superposition of the incident field E_0 and the induced field E_{sp}.

$$E_{molecule} = E_0 + E_{sp} \tag{2.10}$$

The ratio of the total field at the position of the molecule to the incident field gives the field enhancement factor $A(\omega)$. It is stronger when the excitation of surface plasmons of the metal sphere is resonant.

$$A(\omega) = \frac{E_{molecule}(\omega)}{E_0(\omega)} \sim \frac{\varepsilon_1(\omega) - \varepsilon_2}{\varepsilon_1(\omega) + 2\varepsilon_2} \left(\frac{r}{r+d}\right)^3 \tag{2.11}$$

The electromagnetic enhancement factor for the total Stokes signal, $G_{em}(\omega_s)$, is

$$G_{em}(\omega_s) = |A(\omega_s)|^2 |A(\omega_L)|^2 \sim \left|\frac{\varepsilon_1(\omega_L) - \varepsilon_2}{\varepsilon_1(\omega_L) + 2\varepsilon_2}\right|^2 \left|\frac{\varepsilon_1(\omega_s) - \varepsilon_2}{\varepsilon_1(\omega_s) + 2\varepsilon_2}\right|^2 \left(\frac{r}{r+d}\right)^{12} \quad (2.12)$$

From this equation, we can see that the overall enhancement scales with E^4 and it decreases with increasing distance d, resulting in $1/d^{12}$. For single gold and silver nanoparticles the maximum electromagnetic enhancement is in the order of $10^6 - 10^7$. It is evaluated to be in the order of 10^{11} for the gap between two gold or silver spherical particles separated by 1 nm distance [30].

2.2. Resonant coupling

Resonant coupling occurs if the molecule exhibits a strong light absorption around the plasmon resonance energy. This coupling can be weak or strong depending on the distance between the plasmonic particle and the molecule as well as the electronic structure of the two. In this section, background for the resonant SERS, surface-enhanced fluorescence (SEF), plasmon enhanced FRET, and strong coupling are described.

2.2.1. Resonant-SERS

As described in previous section, the electromagnetic enhancement of SERS is strong when the excitation and scattered fields are in resonance with the surface plasmons [30]. If the electronic transitions of the molecule are close to laser excitation energy, the signal becomes stronger. This is called surface-enhanced resonance Raman scattering (SERRS) [31].

Exchange-coupled SERS

Large SERS enhancements were observed when a single Rhodamine 6G is adsorbed on silver nanoparticles. These enhancements cannot be predicted only by electromagnetic enhancement [32]. Classical electromagnetic models only predict enhancement 10^{10} fold. They do not take into account the electronic structure of the molecule and molecule-plasmon interactions [33]. Therefore, there are missing enhancement factors, which are considered to originate from ‘chemical’ or ‘electronic’ effects [30]. According to one view, other SERS enhancement effects can be classified as ground state chemical mechanism (non resonant), molecular resonant mechanisms, and charge transfer mechanism [33]. The molecular resonant Raman enhancement takes place in the case of the excitation wavelength overlaps with the optical absorption of the molecule [7]. The charge transfer resonance enhancement occurs when the excitation wavelength is in resonance with molecule-plasmon charge transitions and only when the distance between molecule and metal is small, and when molecule-plasmon wavefunctions strongly overlap [33]. All of these effects modify the molecular electronic structure compared to that of a non-interacting molecule

[7]. It is hypothesized either the electronic states of the molecule are shifted and broadened or new electronic states appear. According to another view, a charge transfer between the molecule and the metal nanoparticle can occur at around half of the intrinsic intramolecular excitation energy if the highest occupied molecular orbital (HOMO) and the lowest unoccupied molecular orbital (LUMO) of the molecule are evenly positioned in energy compared to the Fermi level of the metal, [34].

2.2.2. Surface-enhanced fluorescence (SEF)

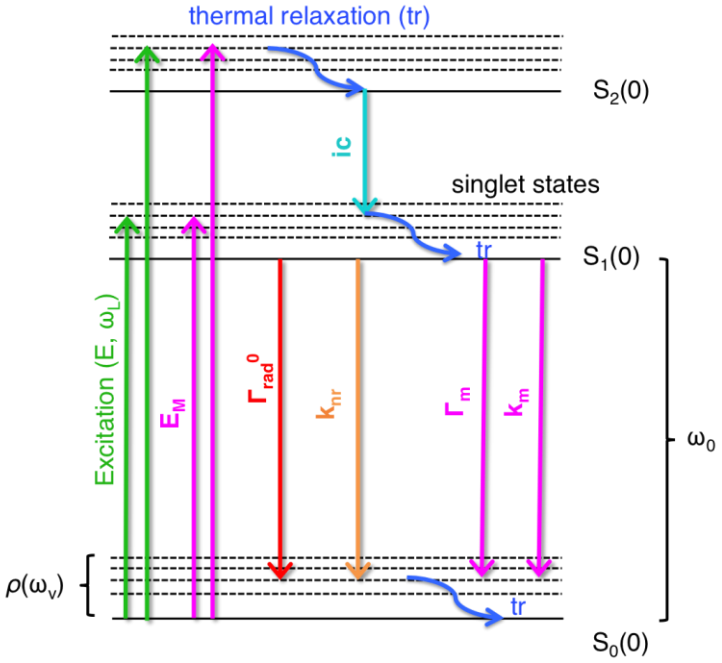

Figure 2.3. Jablonski energy level diagram of a fluorescent molecule and modifications by the nearby metal (shown with pink arrows) [35,36].

When an isolated molecule (with absorption cross section, σ_{abs}^{0}) is excited by a laser at energy ω_L and with a photon flux n_L, the total number of absorbed photons is equal to [21]

$$n_{abs}^{0} = \sigma_{abs}^{0}(\omega_L) n_L \tag{2.13}$$

If an electron is excited from the $S_0(0)$ to the S_1 state and relaxes to the $S_1(0)$ state, then it may radiatively decay to one of the S_0 states, $S_0(\omega_v)$, emitting a photon with a Stokes shift, $\omega_s = \omega_0 - \omega_v$. The total rate for $S_1(0) \rightarrow S_0(\omega_v = \omega_0 - \omega)$ transition is $\gamma_{Tot}^{0}(\omega_s) d\omega_s$ and the overall decay rate becomes

$$\Gamma_{Tot}^{0} = \int \gamma_{Tot}^{0}(\omega_s) d\omega_s \tag{2.14}$$

This total rate consists of radiative, $\gamma_{Rad}^{0}(\omega_s)d\omega_s$ and nonradiative, $\gamma_{NR}^{0}(\omega_s)d\omega_s$, contributions. The radiative decay rate is

$$\Gamma_{Rad}^{0} = \int \gamma_{Rad}^{0}(\omega_s)d\omega_s \tag{2.15}$$

The spectral density of radiated power (number of photons per unit time per Stokes frequency) is then given as the following

$$\mathrm{n}_{Rad}^{0}(\omega_s) = \frac{\gamma_{Rad}^{0}(\omega_s)}{\Gamma_{Tot}^{0}}\sigma_{abs}^{0}(\omega_L)n_L \tag{2.16}$$

This fluorescence spectrum of the molecule depends on $\gamma_{Rad}^{0}(\omega_s)$, which is determined by the density of states $\rho(\omega_0 - \omega_s)$ in the S_0 state. The quantum yield (Q) and the lifetime (τ_0) of an isolated fluorophore are also related with its radiative (Γ_{Rad}^{0}) and non-radiative decay (k_{nr}) rates [35]

$$Q = \frac{\Gamma_{Rad}^{0}}{\Gamma_{Rad}^{0} + k_{nr}} \tag{2.17}$$

$$\tau_0 = \frac{1}{\Gamma_{Rad}^{0} + k_{nr}} \tag{2.18}$$

In the vicinity of plasmonic metal surfaces, the fluorescence intensity and the lifetimes can be modified due to quenching or enhancement by a change in the excitation and emission rates (assuming that there is no modification in the molecular energy levels). The excitation rate at the position of the molecule can be modified due to the enhanced local electric field ($E + E_M$). This gives rise to a modification in absorption by a local field enhancement factor $M_{Loc}(\omega_L)$ and only changes the brightness of the molecule without affecting the quantum yield or lifetime of the molecule [35]. The emission rate can be altered due to local photonic density of states by a factor $M_{Tot}(\omega_s) = M_{Rad}(\omega_s) + M_{NR}$. $M_{NR}(\omega_s)\gamma_{Rad}^{0}d\omega_s$ is the decay rate of the emission into the nonradiative channels, such as absorption by the metal, and $M_{Rad}(\omega_s)\gamma_{Rad}^{0}d\omega_s$ is the modified radiative decay rate [23]. Additionally, there is the intrinsic nonradiative rate $\gamma_{NR}^{0}d\omega_s$, but it is negligible with respect to $M_{NR}(\omega_s)\gamma_{Rad}^{0}d\omega_s$. Consequently, the modified overall decay rate for $S_1(0) \rightarrow S_0(\omega_v = \omega_0 - \omega)$ becomes

$$\Gamma_{Tot} = \int M_{Tot}(\omega_s)\gamma_{Rad}^{0}(\omega_s)d\omega_s = \bar{M}_{Tot}\Gamma_{Rad}^{0} \tag{2.19}$$

and the modified spectral density of radiated power is

$$n_{Rad}(\omega_s) = \frac{M_{Rad}(\omega_s)\gamma^0_{Rad}(\omega_s)}{\Gamma_{Tot}} M_{Loc}(\omega_L)\sigma^0_{abs}(\omega_L)n_L \tag{2.20}$$

Then, the fluorescence spectral enhancement factor can be written as

$$M_{Fluo}(\omega_s) = \frac{n_{Rad}(\omega_s)}{n^0_{Rad}(\omega_s)} = \frac{M_{Rad}(\omega_s)}{\bar{M}_{Tot}} M_{Loc}(\omega_L) \tag{2.21}$$

where $M_{Rad}(\omega_s)$ represents the resonance due to localized surface plasmons, which enables strong fluorescence enhancement with overlapping plasmon resonance and fluorescence emission.

The quantum yield, Q_m, and the lifetime of the molecule, τ_m, are also modified as follows:

$$Q_m = \frac{\Gamma^0_{Rad} + \Gamma_m}{\Gamma^0_{Rad} + \Gamma_m + k_{nr} + k_m} \tag{2.22}$$

$$\tau_m = \frac{1}{\Gamma^0_{Rad} + \Gamma_m + k_{nr} + k_m} \tag{2.23}$$

As illustrated in Figure 2.3, Γ_m is the additional radiative and k_m is the additional non-radiative decay rate due to plasmonic nanostructure. An increase in radiative rates results increased quantum yields and decreased lifetimes.

2.2.3. Plasmon enhanced FRET

Another example of molecule-plasmon interaction is plasmon enhanced Förster (alternatively, fluorescence) resonance energy transfer (FRET), where the near-field plasmon resonance of metal nanostructures can couple to molecules in the vicinity. FRET is a nonradiative energy transfer from a donor molecule in the excited state to an acceptor molecule in the ground state through the dipole–dipole interaction. FRET is limited to certain distance between the donor and the acceptor molecules (around 0.5 - 10 nm). Therefore, the FRET efficiency is highly dependent on the donor-acceptor separation distance. The rate of energy transfer between the two fluorophores, k_{FRET}, is determined by the fluorescence lifetime of the donor without the acceptor, $1/\tau_D^{-A}$, the distance between the fluorophores, R, and the characteristic distance, R_0 [36].

$$k_{FRET} = \frac{1}{\tau_D^{-A}}\left(\frac{R_0}{R}\right)^6 \tag{2.24}$$

The characteristic Förster distance is defined as the separation between the donor and the acceptor when the FRET efficiency is 50%. It is proportional to the

spectral overlap integral of the donor emission spectrum with the acceptor absorption spectrum, J, the quantum yield of the donor in the absence of the acceptor, Q_0, the dipole orientation factor, κ^2, the refractive index of the medium, n, and Avogadro's number, N_A.

$$R_0^6 = \frac{9Q_0 \ln(10)\, \kappa^2 J}{128\pi^5 n^4 N_A} \tag{2.25}$$

The spectral overlap integral equation, contains contributions of the donor's emission spectrum, $f_{D,em}$, and the acceptor's absorption spectrum, $f_{A,abs}$.

$$J = \int f_{D,em}\,(\lambda) f_{A,abs}(\lambda)\lambda^4 d\lambda \tag{2.26}$$

The FRET efficiency (the quantum yield of the energy transfer) is defined as the ratio of the rate of FRET to the total rate of de-excitation. $1/\tau_D^{+A}$ is the fluorescence lifetime of the donor in the presence of the acceptor.

$$\mathrm{E}_{FRET} = 1 - \frac{1/\tau_D^{-A}}{1/\tau_D^{+A}} = \frac{k_{FRET}}{1/\tau_D^{+A}} = \frac{1}{1 + \left(\frac{R}{R_0}\right)^6} \tag{2.27}$$

In an early theoretical work the energy transfer between two molecules was investigated when the molecules are placed close to a small solid particle [37]. It was shown that the FRET could be enhanced with the assistance of the particle in the transfer process. In the presence of the particle, donor dipole induces multipole moments on the particle which can be much larger than the donor dipole itself. The degree of the enhancement of the dipole depends on the shape of the particle, the location of the molecular dipole with respect to the particle, and the spectral match between the plasmon resonance, and the 'overlap integral J'. First, when the particle dipole is excited, it can couple to the acceptor dipole and modify the energy transfer. Secondly, the presence of the particle introduces new decay channels competing with the energy transfer. Hence, the presence of the particle modifies not only the energy transfer rate, but also the radiative and non-radiative decay rates of the donor and acceptor molecules. From the given parameters above, we know that the quantum yield of the donor and the absorption coefficient of acceptor should be high enough for a significant probability of the transfer, which only takes place in a limited distance between the fluorophores [36]. Plasmonic nanostructures have potential to enhance the characteristic Förster distance by improving the quantum yield of the donor and the excitation of the acceptor [38].

The Figure 2.5 shows some of our preliminary results of enhancing FRET and/or acceptor emission by using plasmonic nanostructures for the ratiometric FRET imaging in mammalian cells. MT1-MMP (membrane type 1 matrix metaloproteinase) is a membrane-anchored enzyme, known to be crucial during cancer invasion and metastasis. It is observed in a broad range of human cancers in clinical examples. MT1-MMP is tagged by orange and red fluorescent proteins in order to have simultaneous visualization of a MT1-MMP in addition to another FRET biosensor which is tagged by the most commonly used FRET pair cyan-yellow fluorescent proteins [39]. Figure 2.4 gives the schematic diagram of the FRET sensor and both absorption and emission spectra of donor and acceptor fluorescent molecules.

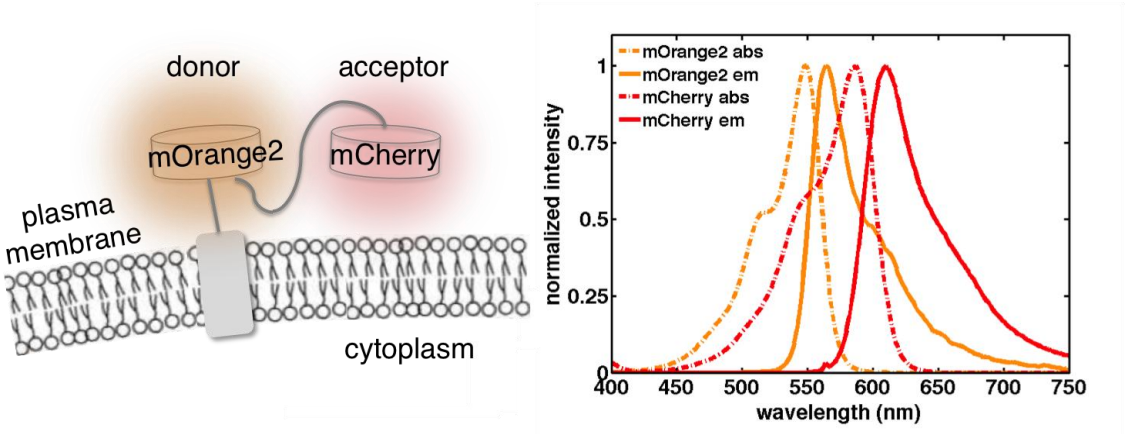

Figure 2.4. On the left, a schematic diagram of the FRET biosensor is given. The absorption (dashed lines) and emission (solid lines) spectra of donor (mOrange2) and acceptor (mCherry) fluorescent proteins are shown in the graph. Intensities are normalized [39].

In this system, the acceptor molecule, (mCherry) exhibits a quite low quantum yield, of 0.2. This makes the pair inefficient for ratiometric FRET imaging, a widely used method to measure FRET in biological applications. It is based on separate imaging of the donor and the acceptor channels, and subsequent division of one channel by the other to generate the ratio image. In our case, the acceptor channel is divided by the donor channel as shown in Figure 2.5.

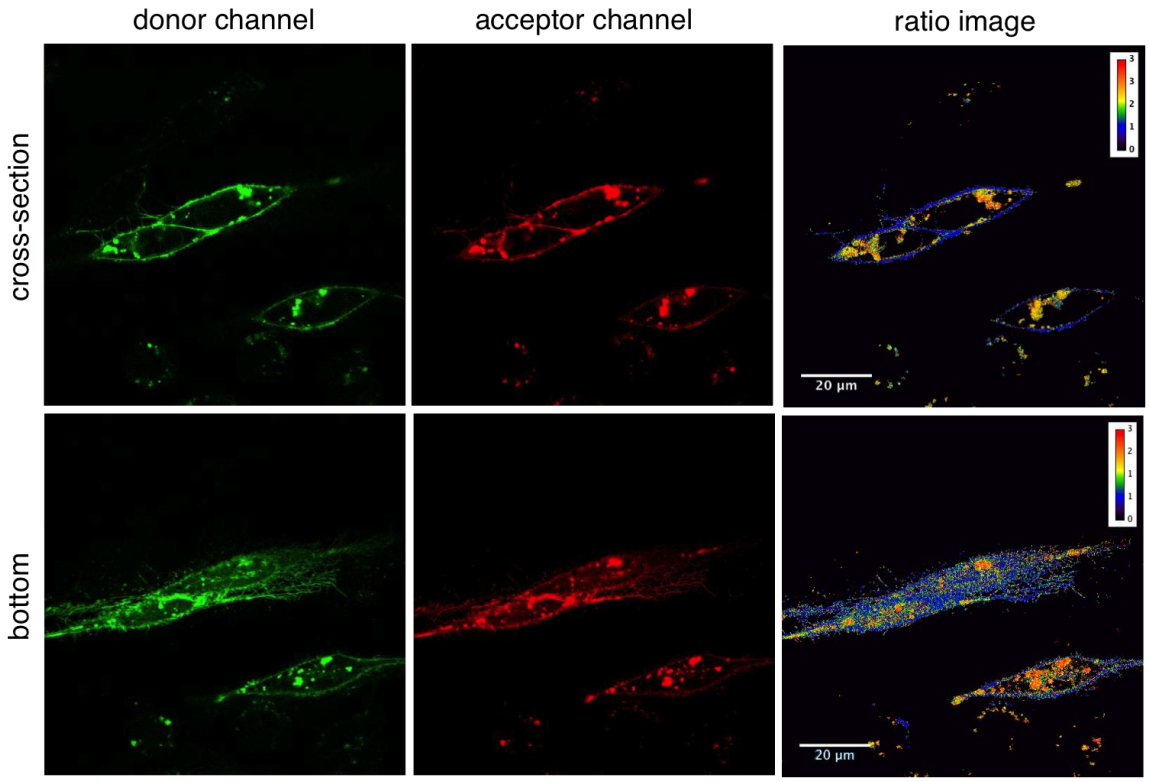

Figure 2.5. Confocal microscopy images of live HeLa cells expressing MT1-MMP FRET biosensor on a cover glass. The images in the first row show the cross-section of the two attached cells and the images in thee second row show the bottom part of the plasma membrane. The green images are from the donor channel, the red images are from the acceptor channel, and the last column images are ratio images (acceptor/donor).

Our aim is to improve ratiometric imaging by using plasmonic nanoparticles. Figure 2.6 shows the concept our experiments. HEK293 (Human Embryonic Kidney 293) cells expressing the MT1-MMP biosensor are grown on three different plasmonic substrates. Substrate 1 is tuned in such way that the plasmon resonance peak matches the donor emission and the acceptor absorption. Substrate 2 is designed such that the plasmon peak overlaps the emission of the acceptor. The other substrate is the control, a simple cover glass without any particles. For each substrate, 20-25 fluorescence images were collected under the same imaging conditions and parameters. Ratio images were processed according to the described algorithm [40]. The integrated intensity was calculated for each image, and then averaged for the total number images, giving the averaged integrated intensity. Preliminary results of the experiment are shown in Figure 2.7. Substrate 1 shows a higher intensity in ratio images compared to the control substrate. This substrate led to a higher intensity in the acceptor channel and a lower intensity in the donor channel, possibly due to enhanced energy transfer. However more experiments need be done in order to analyse the results more quantitatively (e.g. calculate the transfer efficiencies) and to understand the mechanism behind these results.

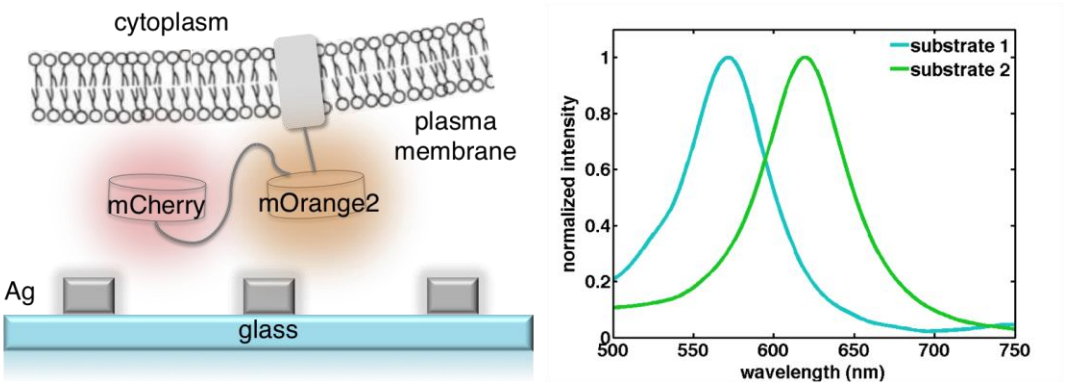

Figure 2.6. On the left, a schematic diagram showing the mammalian cells expressing the FRET biosensor on the substrates. On the right, normalized absorption spectra of two different substrates measured in water. Substrate 1 exhibits the plasmon peak at 572 nm, overlapping with donor emission and acceptor absorption spectra. The substrate 2 shows a plasmon peak at 620 nm, that overlaps with acceptor emission spectrum.

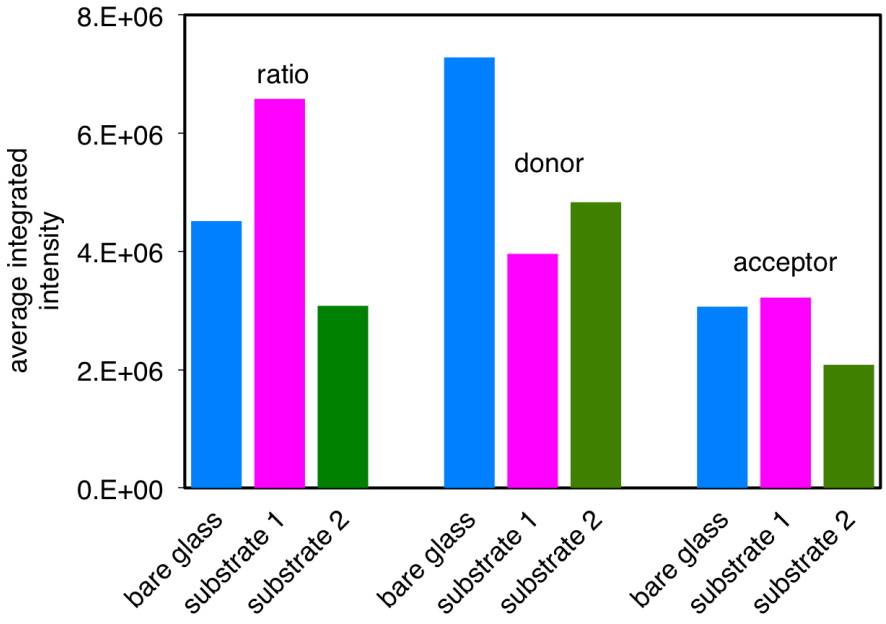

Figure 2.7. Chart showing the average integrated intensities for different substrates for the donor, acceptor, and ratio images. For each substrate, the integrated intensity was calculated from single cell images and averaged for 20-25 cell images.

2.2.4 Strong coupling

The strong coupling between molecules and plasmons has been interpreted from many different perspectives. Therefore, it is possible to come across a wide range of terminologies to explain the phenomenon, such as hybridization, plasmon splitting, electromagnetically induced transparency, and plasmon resonance energy transfer. According to Halas et al. [41], when a quantum emitter is placed near a plasmonic nanostructure, the electromagnetic interaction between the surface plasmon and the exciton can result in hybridized states. The wavefunctions of these hybridized states are interpreted as the combination of the exciton and the plasmon mode, and these states consist of bonding and antibonding states.

According to another perspective, the strong coupling interaction can be described by energy transfer between the molecule and the plasmon [42]. For instance, Förster resonant energy transfer (FRET) is considered as a weak coupling between donor and acceptor molecules. FRET assumes that the transfer rate from donor to acceptor is smaller than the relaxation rate of the acceptor, so that once the energy is transferred to the acceptor, there is a low possibility of reverse transfer to the donor. When the interaction energy becomes large enough, a reverse transfer to the donor becomes possible, and the system shifts into the strong coupling regime. In this regime, donor and acceptor become indistinguishable, and the molecule-plasmon pair is considered as one system. In a similar manner, plasmon resonance energy transfer (PRET) between plasmonic nanostructures and molecules is another interpretation of strong coupling [26]. In analogy with the FRET, where the donor emission and acceptor absorption has to overlap in energy, for PRET a match between the plasmon resonance and the electron transition energy of the molecule is needed, and energy is possibly transferred through the dipole-dipole interaction between the resonating plasmon dipole and the molecular dipole.

Plasmonic splitting is another perspective in strong coupling literature, which is observed as two or more resonance peaks in the spectrum of the particle, depending on the number of the absorption bands of the molecule [43]. It is considered as analogy to the Rabi splitting in quantum mechanical systems. From this point of view, the plasmonic splitting takes place because of an exchange of photons between the plasmonic nanoparticle and the dye molecules. Such a mechanism can win over decoherence sources and can result in new coherent hybrid states.

It was also claimed that by varying the oscillator strength and molecular transition line width, either plasmonic splitting or a quenching of dips could be observed on the spectrum of the dye molecule coated plasmonic nanoparticles [43]. According to the authors, the plasmonic energy transfer described by quenching dips at the position of the molecular absorption band happens when both the oscillator strength and the line width of the molecular transition of the dye is small. For a

large line width, overall quenching can be observed. On the contrary, the plasmonic splitting occurs when both the oscillator strength and line width of the molecular transition of the dye are large.

Energy level splitting is considered as a characteristic feature of the strong coupling interaction and it can be understood from a classical approach [42]. The coupled harmonic oscillators model is an intuitive classical model to explain strong coupling. Here, the surface plasmon resonance and molecular transition are each treated as damped harmonic oscillators, which are the representation of the polarization of the metal nanoparticles and the emitter. These oscillators are coupled to each other through the electric near field with the coupling strength g and the equation of motion are given as [44]:

$$\ddot{x}_{SP}(t) + \gamma_{SP}\,\dot{x}_{SP}(t) + \omega_{SP}^2\,x_{SP}(t) + g\dot{x}_E(t) = F_{SP}(t) \tag{2.28}$$

$$\ddot{x}_E(t) + \gamma_E\,\dot{x}_E(t) + \omega_E^2\,x_E(t) - g\dot{x}_{SP}(t) = F_E(t) \tag{2.29}$$

In these equations x_{SP} and x_E are the coordinates of the surface-plasmon and emitter oscillations, ω_{SP} and ω_E the centre frequencies, γ_{SP} and γ_E are the linewidths, and F_{SP} and F_E are the driving normalized forces because of the external electromagnetic field. The emitter excitation by itself is insignificant with respect to the metal nanostructures, therefore the driving force for the emitter can be neglected. If the applied light has the frequency ω and the driving force is $F_{SP}(t) = \mathrm{Re}\left(F_{SP}\,e^{-i\omega t}\right)$, the steady state coordinates are expressed as the following:

$$x_{SP}(t) = Re\left(\frac{\left(\omega_{QD}^2 - \omega^2 - i\gamma_{QD}\omega\right)F_{SP}(t)}{(\omega^2 - \omega_{SP}^2 + i\gamma_{SP}\omega)(\omega^2 - \omega_E^2 + i\gamma_E\omega) - \omega^2 g^2}\right) \tag{2.30}$$

$$x_{QD}(t) = Re\left(\frac{-ig\omega F_{SP}(t)}{(\omega^2 - \omega_{SP}^2 + i\gamma_{SP}\omega)(\omega^2 - \omega_E^2 + i\gamma_E\omega) - \omega^2 g^2}\right) \tag{2.31}$$

The total extinction cross-section of the structure, C_{ext}, including both absorption and scattering can be calculated from the work done by the applied force.

$$C_{ext}(\omega) \propto \langle F_{SP}(t)\dot{x}_{SP}(t)\rangle \tag{2.32}$$

$$C_{ext}(\omega) \propto \omega\, Im\left(\frac{(\omega_E^2 - \omega^2 - i\gamma_E\omega)}{(\omega^2 - \omega_{SP}^2 + i\gamma_{SP}\omega)(\omega^2 - \omega_E^2 + i\gamma_E\omega) - \omega^2 g^2}\right) \tag{2.33}$$

Even though the scattering cross-section cannot not be calculated in a straightforward way by the coupled-oscillator model, it is still possible to calculate

it in quasi-static limit where $k = \frac{\omega n}{c}$ is the wavevector of light and α is the polarizability of the plasmonic nanostructure.

$$C_{ext}(\omega) = 4\pi k Im(\alpha) \tag{2.34}$$

By using these two equations, the scattering cross-section can be written as

$$C_{sca}(\omega) = \frac{8\pi}{3} k^4 |\alpha|^2 \tag{2.35}$$

$$C_{sca}(\omega) \propto \omega^4 \left| \frac{(\omega_E^2 - \omega^2 - i\gamma_E \omega)}{(\omega^2 - \omega_{SP}^2 + i\gamma_{SP}\omega)(\omega^2 - \omega_E^2 + i\gamma_E \omega) - \omega^2 g^2} \right|^2 \tag{2.36}$$

In Figure 2.8 (b) the calculated scattering spectrum of a spherical silver particle coupled with Rhodamine 6G according to the coupled harmonic oscillator model is shown. For this calculation, the experimental Rhodamine 6G absorption spectrum is fitted with 2 Lorentzian functions as it exhibits two dominant peaks at 500 nm and 531 nm (a). In the coupled harmonic oscillator model, each of these peaks is coupled to surface plasmon independently.

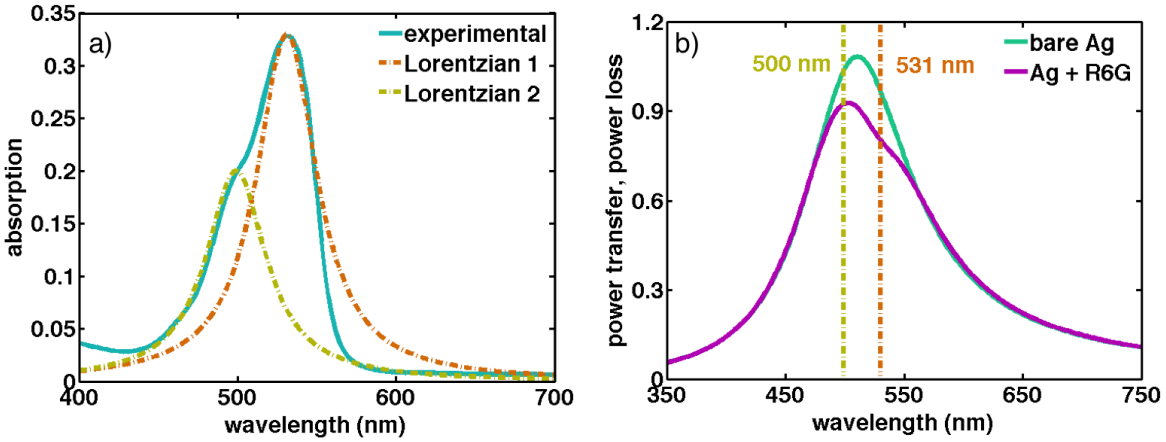

Figure 2.8. Absorption spectrum of thiolated Rhodamine 6G. It shows two distinct peaks at 531 nm and 500 nm (a). Spectrum of an uncoated single Ag spherical nanoparticle and one coated with thiolated Rhodamine 6G (b).

A strongly interacting system can be characterized by an anti-crossing behaviour. A system that consists of two coupled oscillators can be identified by two natural frequencies. When the coupling between the oscillators strengthens, the energy separation (energy splitting) between these two oscillators increases. This can be considered as repulsion between the frequencies, as the lower frequency decreases and the higher increases. This anticrossing in energy with a

separation is known as vacuum-Rabi splitting. An example of anti-crossing behaviour for a metal spheroid coated with a resonant molecule is illustrated in Figure 2.9 in the extinction spectrum [45]. ω_p is the plasmon frequency, ω is the external field frequency, and $\omega_{0\|}$ is the molecular resonance, when the molecules have their resonant axis parallel to the surface normal. The horizontal dashed lines denote two plasmon resonances of the metal spheroid, along its long (x) and short (z) axes. The diagonal dashed line represent the molecular resonance. The high frequency modes correspond to antibonding, which the induced dipole on the particle is out of phase with the molecular transition dipoles. Similarly, low frequency modes correspond to bonding, which the excitations are in phase. In order to enter strong coupling regime, the splitting needs to be larger than the sum of the linewidths. This indicates that the dissipation in each oscillator has to be smaller than the coupling strength [42]. In order to have strong coupling either the coupling strength needs to be made as large as possible or decoherence effects need to be reduced.

$$\frac{\Gamma}{\frac{\gamma_{SP}}{m_{SP}} + \frac{\gamma_E}{m_E}} > 1 \qquad (2.37)$$

It was also reported that the splitting energy varies with the square root of the absorbance, which itself depends on the film thickness, the concentration, and intrinsic absorption cross section of the dye molecule [46].

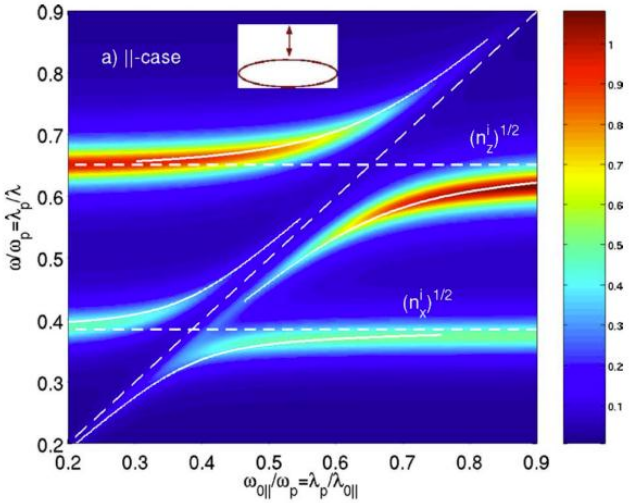

Figure 2.9. An example of anticrossing behaviour between the plasmonic and molecular resonances. This figure corresponds to strong coupling in a metal spheroid coated with a resonant molecular shell. The molecule has its resonance parallel to the surface normal [45]. fgfgf

Chapter 3

Methods and Characterization

In this chapter, general background about the material, sample preparation, and characterization methods used in attached papers are presented. In both Paper 1 and Paper 2, silver colloidal (BBI Solutions) particles stabilized by citrate were used. In Paper 1 colloidal Ag particles are coated with thiolated Rhodamine 6G and Paper 2 is about colloidal Ag nanorods coated with J-aggregates. The details of how to coat Ag particles by the dyes are given in the attached papers, along with the details about the equipment and parameters used.

3.1. Sample preparation

3.1.1. Self-assembled monolayers (SAM)

There are different ways of immobilizing fluorescent emitters on metal surfaces, like through physical and chemical interactions One of the most common immobilization methods is the adsorption of molecules on metal surfaces via organic thiol chemistry. Thiols have strong affinity towards noble metal surfaces. With thiol chemistry, it is possible to engineer organic surfaces on metal surfaces with various chemical functionalities [47]. For example, thiols such as alkanethiols can adsorb on gold (Au), silver (Ag), and copper (Cu) and form self-assembled monolayers. The adsorption of thiols on these metals show structural differences due to the differences in reactivity of the surface of the metal (i.e. especially oxidation of the surface) [48].

3.1.2. J-aggregates

In 1930s, Scheibe and Jelley independently observed an interesting behaviour in pseudoiso-cyanine chloride (PIC). When the concentration of the PIC dye is increased (above around 1 – 10 mM) in aqueous solution, the peak position of absorption of the dye shifted towards higher wavelengths. The full width at half maximum (FWHM) narrows. The absorption coefficient increases thereby amplifying strong fluorescence emission with a small Stokes shift [49]. Figure 3.1 shows the absorption spectra of PIC chloride aggregates in water (the solid line) and PIC chloride monomers in ethanol (the dashed line). In the inset the structure of PIC chloride is given.

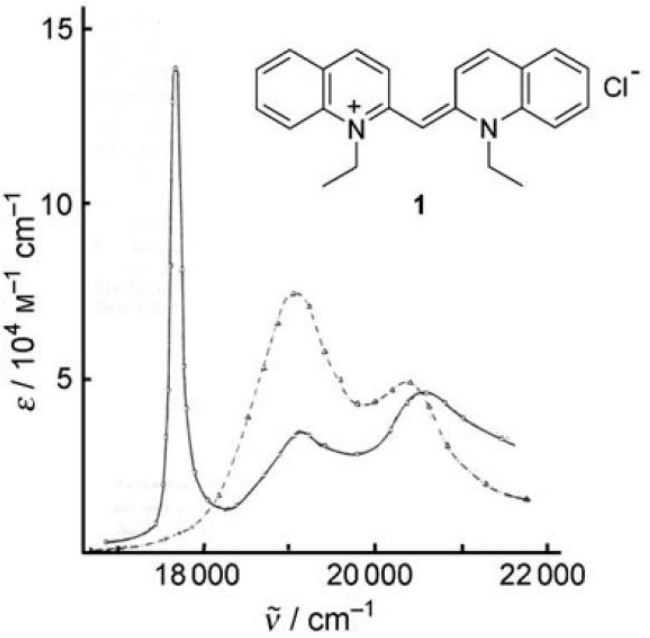

Figure 3.1 Absorption spectra of PIC chloride monomers in ethanol (the dashed line) and the aggregates in water (the solid line). Inset shows the structure of the PIC molecule [49].

Similar spectral effects were observed in aqueous solutions of the PIC dye upon increasing NaCl concentration, which leads to screening of electrostatic charges and thus promotes aggregation. These spectral changes were interpreted as the result of the dye polymerization and are called either Scheibe aggregates or J-aggregates (J denoting Jelley) according to the name of the inventors. If the aggregates have absorption band shifted towards blue wavelengths, they are called H-aggregates (H denoting hypochromic). These aggregates usually show low or no fluorescence emission. Different possible arrangements of dye molecule aggregates such as brickwork, ladder, or staircase arrangements have been suggested [49]. Among these models, the brickwork arrangement was considered to be the most likely arrangement of monomers in PIC J-aggregates. Later, a threaded double-string model was proposed, which may be interpreted as a subunit of the brickwork model. Another suggested model was threadlike aggregates composed of two monomers per unit length. Even though the true nature of aggregate molecules is still under investigation, head-to-tail arrangement of monomers to form J-aggregates, the parallel arrangement of monomers to form sandwich type aggregates, H-aggregates, are considered. Figure 3.2 shows the energy states of inter-molecule coupling for head-to-tail and parallel oriented molecules. When two molecules are close to each other, their transition moments interact to form two new energy states. In Figure 3.2 the dashed lines represent forbidden transitions. According to molecular exciton theory described in [50], if molecules oriented in the head-to-tail configuration exhibit an in-phase arrangement, the transition dipoles causes an electrostatic attraction and therefore a lower energy state. Similarly, an out-of-phase

arrangement leads to electrostatic repulsion and a higher energy state. Consequently, an in-line transition dipole state results in the strong spectral red shift with respect to monomer due to the lowering in energy. Likewise, electronic transitions in parallel dimers is blue shifted with respect to electronic transitions in monomers. Both in head-to-tail and parallel configurations, the in-phase arrangement leads to larger dipole moments and stronger absorption compared to the monomer case.

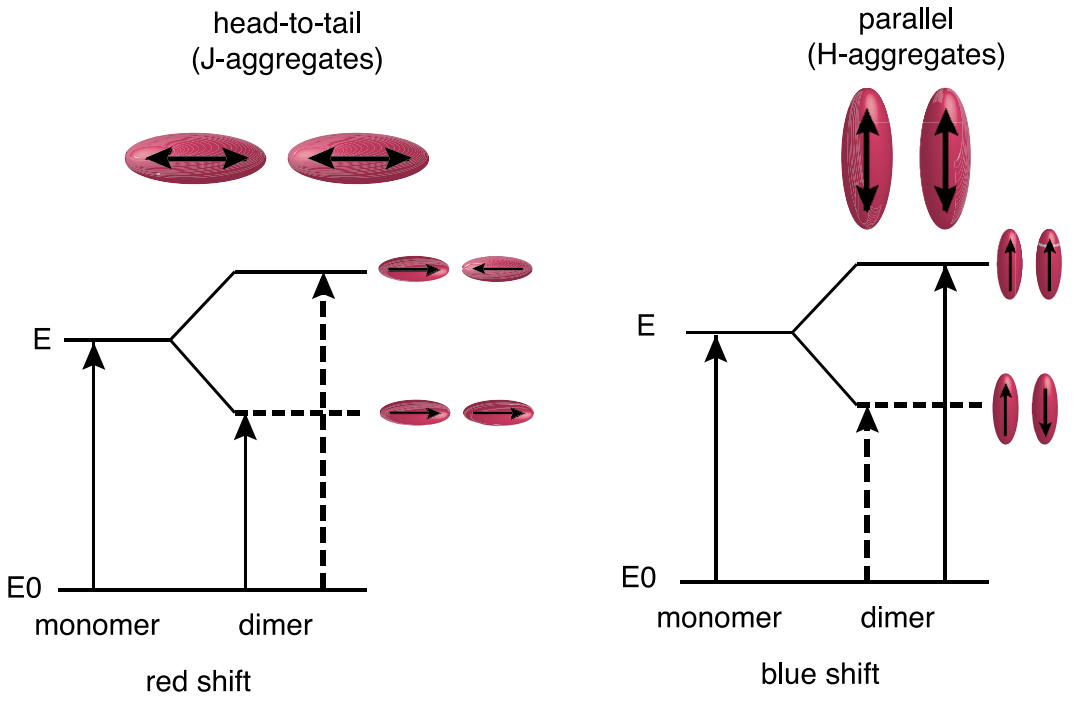

Figure 3.2 Exciton splitting of dimers in different configurations. Orientations of the dipoles are shown by the arrows [50,51].

In Paper 2, TDBC J-aggregate dye was used. Its monomer and J-aggregate absorption spectra are given in Figure 3.3 [52].

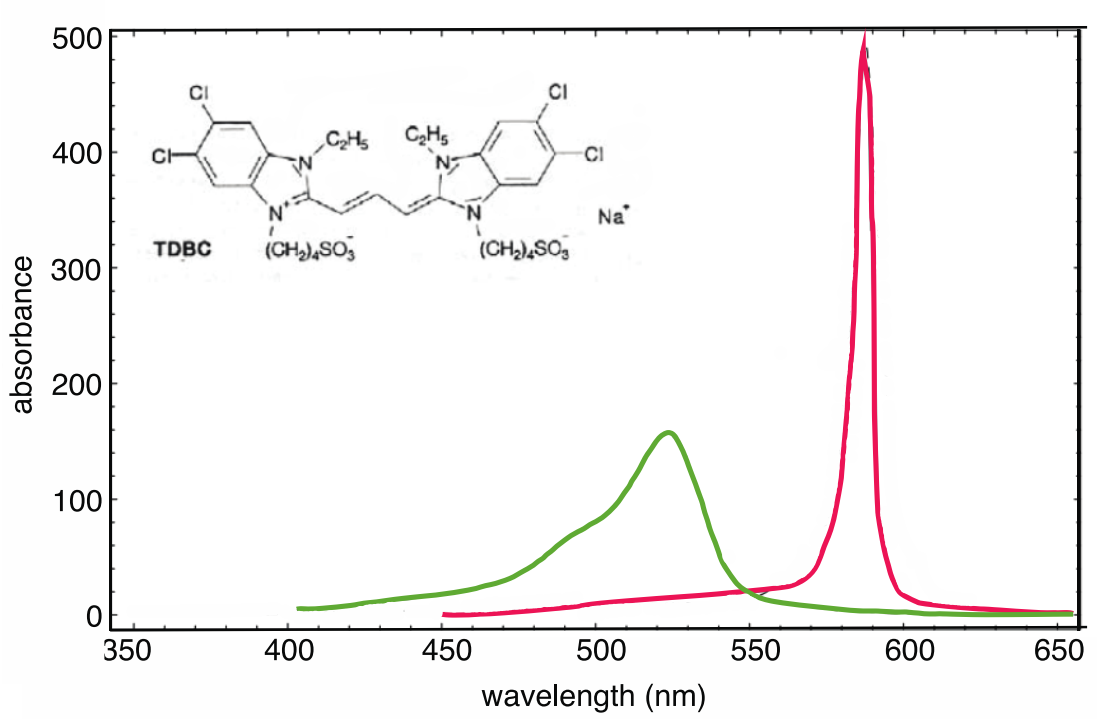

Figure 3.3 The absorption spectra of TDBC dye in monomer (green curve) and J-aggregate (red curve) forms. The inset shows the structure of the dye adapted from [52].

3.1.3. Tween 20

Polyoxyethylene (20) sorbitan monolaurate, also called Tween 20, is a nonionic surfactant used to prevent irreversible aggregation upon chemisorption of alkanethiols on colloidal metal nanoparticles. In Paper 1, colloidal Ag nanoparticles were coated with thiolated Rhodamine 6G in the presence of Tween 20. The physical adsorption of Tween 20 onto metal nanoparticles prior to adsorption of thiol stabilizes the particles against aggregation by the oligo(ethylene glycol) subgroup of Tween 20 [53]. The interaction between metal (Au/Ag) surfaces and Tween 20 is weaker than the interaction between metal surfaces with alkanethiols (i.e. physisorption versus chemisorption). The weakly adsorbed surfactant could be subsequently displaced by alkanethiols chemisorbing onto the metal surface. Fusion of the metallic cores of particles is one of the mechanisms causing irreversible aggregation of colloidal particles. Tween 20 prevents aggregation by acting as an intermediate layer preventing the fusion of the particles until colloids are completely covered by a monolayer of thiols. Figure 3.4 illustrates the mechanism of Tween 20, namely the prevention of the aggregation of colloidal particles upon binding of thiol to colloidal particles [53].

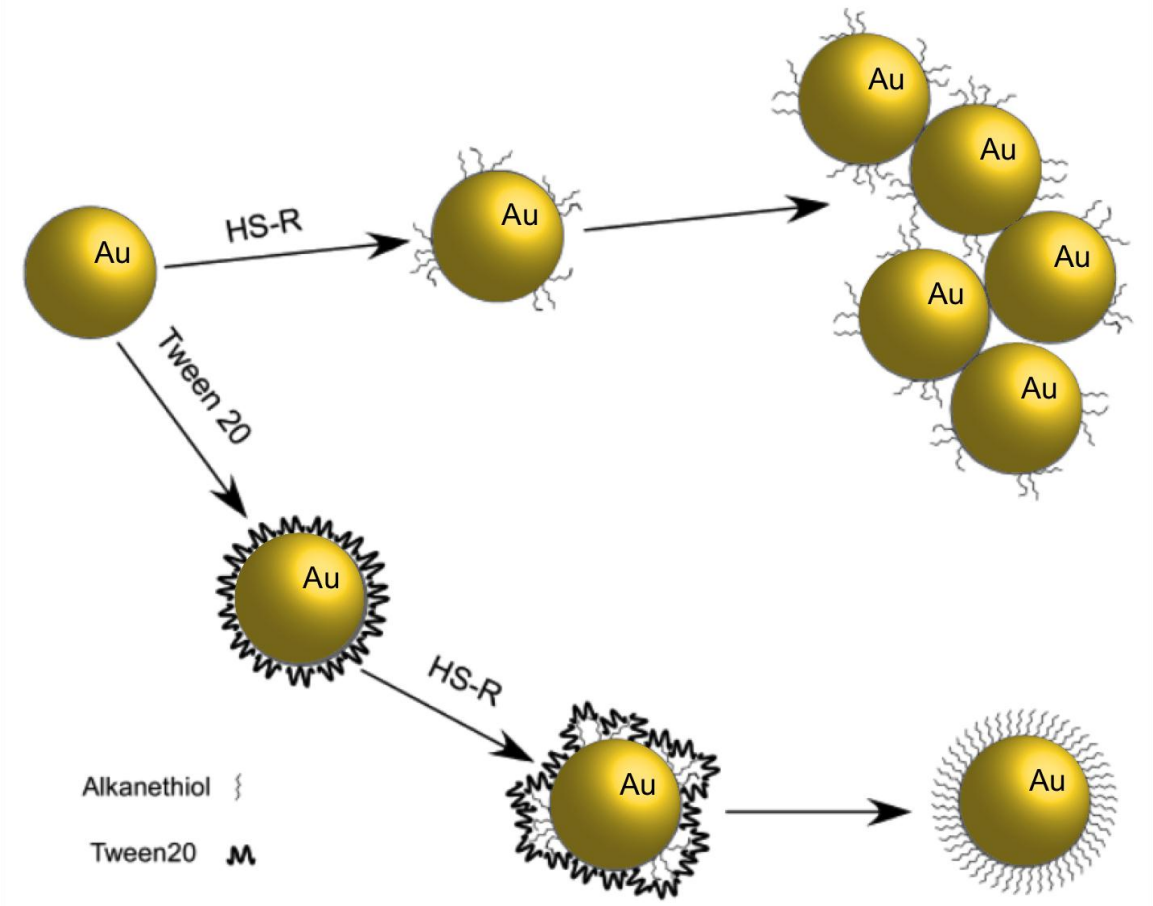

Figure 3.4 Scheme showing the formation of thiols on colloidal Au particle by using tween 20 (adapted from [53]).

3.2. Optical characterization

3.2.1. Dark-field microscopy

Dark field microscopy is a widely used microscopy technique to image unstained samples. This technique is based on blocking the central light along the optical axis that passes through the specimen without scattering. In terms of Fourier optics, 0^{th} order diffraction is removed, such that only oblique rays emerging from scattering of the specimen are collected. This produces an image of bright objects with a dark background, which is constructed from higher order diffraction. The central light is blocked using a specific disk size and remaining light is focused on the sample via a condenser lens. The condenser lens has a higher numerical aperture than the objective, such that the sample is illuminated with a high angle of incidence and only scattered light is collected. While transmission configuration requires transparent samples, non-transparent samples are measured in reflection mode. The Figure 3.5 illustrates the

schematic of dark-field microscopy in transmission mode. The Figure 3.6 shows colloidal Ag nanoparticles on a cover glass, as imaged by dark-field microscopy. In the image, Ag particles have different colours owing to the fact that they scatter light at different wavelengths due to their geometry (e.g. size and shape).

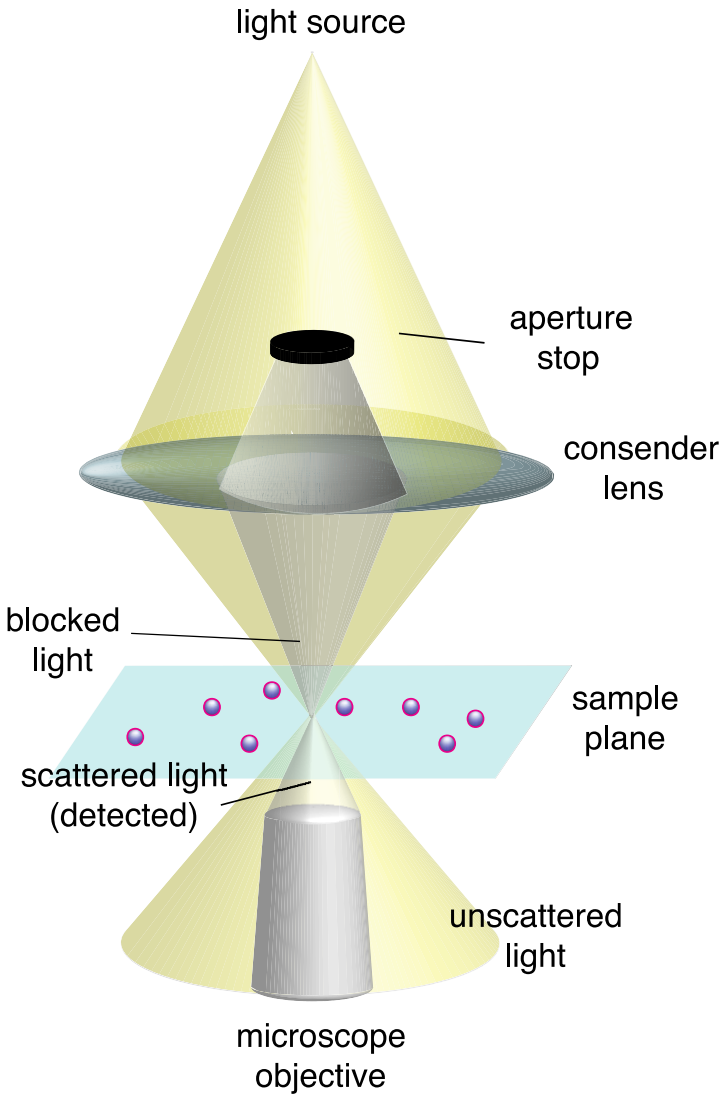

Figure 3.5 Schematic diagrams showing light path of dark field microscope in transmission mode

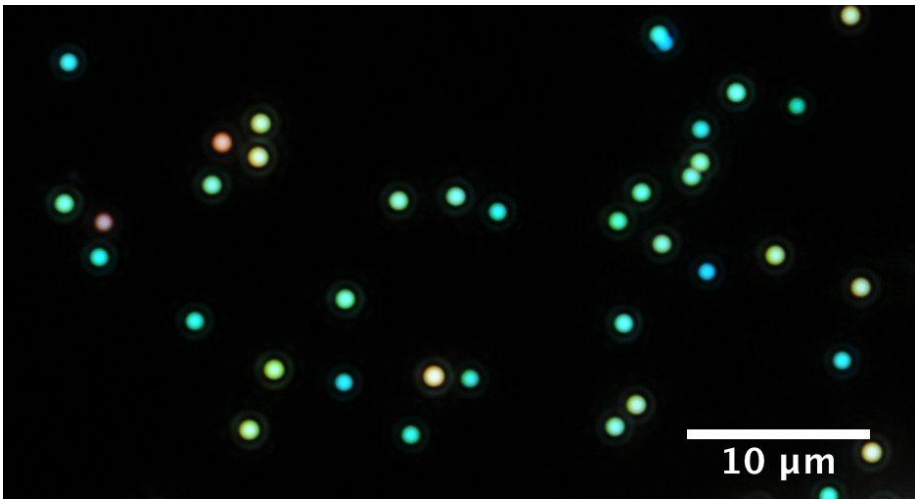

Figure 3.6 Dark field microscopy image of colloidal silver nanoparticles on a glass cover slide.

3.2.2. Fluorescence microscopy

Fluorescence microscopy is another common imaging technique, which uses fluorescence and phosphorescence emission as a contrast signal compared to background. Fluorescence microscopy is based on illuminating fluorophores and collecting the emission light which has higher wavelength than the illumination wavelength. For this purpose, excitation filters, emission filters, and dichroic mirrors are used which are chosen according to excitation and emission spectrum of the fluorophore. The Figure 3.6 shows the basic fluorescence microscopy configuration. The emission filter only allows certain wavelength to enter to the filter cube. Then a dichroic mirror reflects incoming light and directs it towards the objective. Fluorescence emission from the dye is collected by the objective. Objectives with higher numerical apertures are preferred in order to collect more light. Then the light passes through the dichroic mirror then the emission filter. The Figure 3.8 shows a fluorescence microscopy image of Ag colloidal nanoparticles coated by thiolated Rhodamine 6G. As the size and the shape of the particles are different, varying intensity and colour of Rhodamine 6G is observed. This variation is due to the modification of fluorescence by plasmonic nanoparticles.

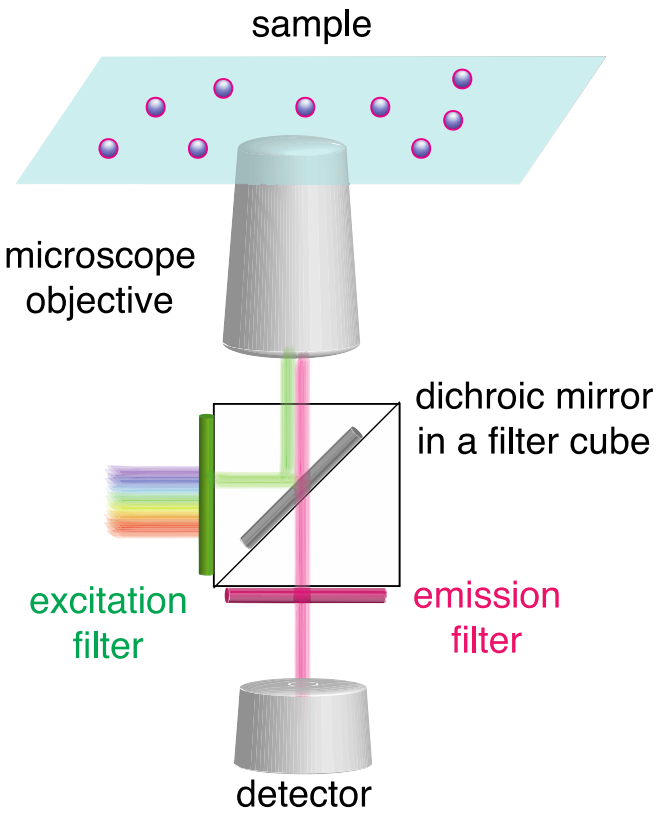

Figure 3.7 Schematic diagrams showing light path of fluorescence microscope

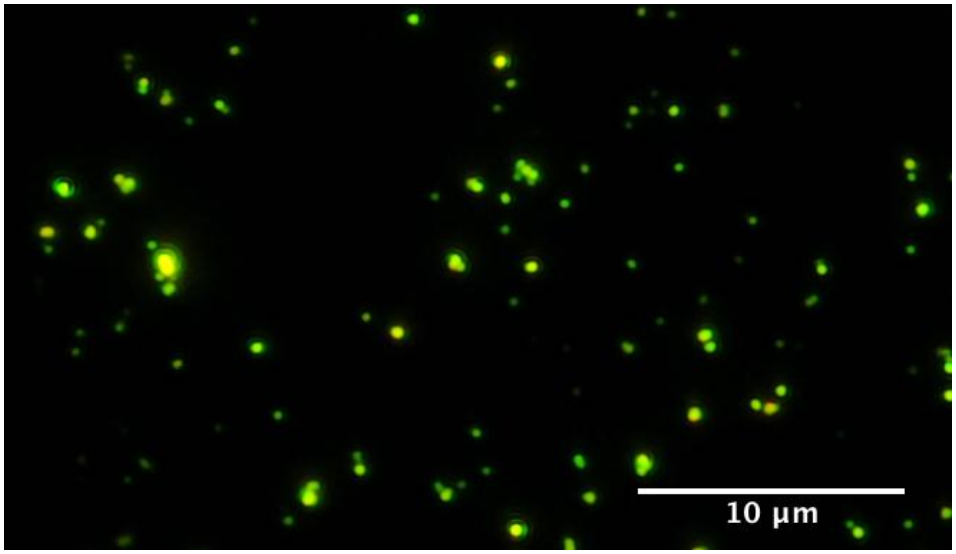

Figure 3.8 Fluorescence microscopy image of colloidal Ag nanoparticles coated by thiolated Rhodamine 6G

Chapter 4

Summary and Outlook

4.1 Summary of appended papers

Paper I, *Interaction between Localized Surface Plasmons and Thiolated Rhodamine 6G: Spectral Dips at Single Particle Level,* is a report about observing dips in the scattering spectra of single silver particles which are coated by Rhodamine 6G. These spectral dips correspond to the wavelengths where Rhodamine 6G has absorption features. Even though Rhodamine 6G has been extensively studied especially in Surface-enhanced Raman Scattering studies, this is a first experimental observation of spectral dips with Rhodamine 6G at single particle level. This observation became possible by using a novel type of Rhodamine 6G that has a thiol end group. Using thiol groups to adsorb Rhodamine 6G on silver surface provides close packing of Rhodamine 6G, which increases the total oscillatory strength of Rhodamine 6G molecules interacting with silver nanoparticles. These spectral dips were measured for many particles and they showed variety in terms of the dip intensity. We attribute the differences in the intensity of the dips to variations in size and shape of the silver particles. Dimer silver particles show stronger dips since electromagnetic field enhancement is higher in dimers compared to single spherical particles. We modelled the Rhodamine 6G coated silver nanoparticles by Mie theory. The calculations suggest that the surface-enhanced absorption of Rhodamine 6G molecules constitutes an important part of the intensity decrease in scattering, while the other contributions can come from the coupling between Rhodamine 6G and silver nanoparticles. This is an important result because in previous studies, similar spectral dips were attributed to only strong coupling between the fluorophore molecule and plasmonic nanoparticles.

Paper 2, *Observation of exciton-induced transparency on a single plasmonic nanoparticle,* is a study of single silver nanorod coated by a shell of J-aggregate cyanine dye. We observed very strong dips in scattering spectra which we attribute to strong interaction between localized surface plasmons of silver nanoparticles and electronic excitations in the J-aggregate molecule. The scattering spectra show about 50% transparency which is the largest dips reported to our knowledge at single particle level. The reason why J-aggregates showed stronger dips in scattering is the high oscillator strength of the molecule, the narrow molecular resonance width, and small silver particle volumes. We studied this coupled molecule-plasmon system with a classical model, where two harmonic oscillators are coupled to each other. We fit this model to scattering spectra of 20 different individual silver nanorods coupled to J-aggregate molecules. The parameters obtained from the model showed an anti-crossing behaviour, which is attributed to a strong coupling regime. Moreover, we

analysed the system by using an analytical model. A core-shell model was used to calculate polarizability of the dye-particle structure. We found that the transparency dips in scattering spectra increase with higher surface to volume ratios of the particles. In other words, smaller particles show less radiative damping and narrower plasmon width, and have more dye molecules per metal atom in the core. This results in a stronger interaction between dye molecules and plasmonic particles.

4.2. Outlook

In Paper 1, we demonstrated results from the interaction of silver nanoparticles with thiolated Rhodamine 6G. As ordinary Rhodamine 6G is a widely used fluorophore (especially with silver surfaces in SERS studies), it is crucial to compare thiolated Rhodamine 6G to ordinary Rhodamine 6G. Therefore we applied the same experimental procedure to ordinary Rhodamine 6G and silver nanoparticles, but the silver particles aggregated with ordinary Rhodamine 6G even in the presence of Tween 20. This shows that thiolated Rhodamine 6G has strong advantage over ordinary Rhodamine 6G not only in terms of having densely packaged molecules on silver particles, but also in sample preparation. However, still more comparative studies between thiolated and ordinary Rhodamine 6G are needed at each level of the sample preparation and characterization.

Thiolated Rhodamine 6G has potential to provide advantage over ordinary Rhodamine 6G in SERS. Thiolation makes the molecule to show specific and selective affinity towards noble metal surfaces. Thus by designing SERS substrates with different materials, it can be possible to densely attach Rhodamine 6G to specific positions on the substrate. For instance, immobilizing Rhodamine 6G specifically on hotspots can enable stronger SERS enhancement factors.

In Paper 2 we showed that it is possible to obtain stronger interaction between plasmonic particle and dye molecules by using smaller plasmonic particles. However, it becomes a challenge to measure single particle scattering in smaller particles due to lower radiative damping. This requires observations in absorption rather than scattering, since absorption becomes the dominant effect. On the other hand, single particle absorption measurements are experimentally difficult. Developing a method which enables single particle absorption measurements would be an important step in this field.

Another future work can be devoted to stabilization of the J-aggregates molecules. As shown in the Figure 3 of Paper 2, J-aggregates breaks up into monomers by laser illumination. Embedding J-aggregate molecules into metal oxide layer could be an option to stabilize the dye. Furthermore, plasmonic structure can be improved to obtain stronger near fields at the position of the dye

molecule. For instance configurations like bow-tie antennas or dimers can show strong coupling in the presence of even smaller number of fluorophores due to enhanced near fields.

Acknowledgements

This thesis became possible with the support of many people. I would like give thanks to

First of all, my supervisor **Mikael Käll** for giving me the opportunity to work in this group. I am grateful for your support with this thesis and the papers.

My co-supervisor **Timur Shegai** for your enthusiasm and support. I learned a lot from you, both in the lab and from our discussions about science.

All the co-authors of the papers. **Tomasz Antosiewicz** for his valuable theoretical contribution and helpful discussions, which gave an important understanding to my experiments. I wish you good luck in Warsaw. **Tina Gschneidtner** and **Kasper Moth-Poulsen** for your nice collaboration.

Malin Bäckström, Elisabeth Thomsson, and **Richard Lymer** for helping with cell cultivation and our discussions. **Julia Fernandez-Rodriguez** and **Maria Smedh** for your help with live cell imaging and fruitful discussion. I learned a lot from all of you.

Joachim Goedhart and **Dorus Gadella** for inviting me to the cell microscopy workshop in Amsterdam, helpful discussions, and providing plasmids.

Peter Johansson, for our discussions about modelling Rhodamine 6G.

Elin Esbjörner Winters, for our discussions about FLIM microscopy.

The whole **Bionanohotonics** group for nice moments all together. **Si**, for our discussions in the lab and training in the clean room. **Virginia**, **Anni**, and **Mitra**, for sharing the office with me, and for our scientific, and non-scientific conversations, and our nice times. **Andreas** for being my new inspiring office mate and answering my questions. I am learning a lot from you. **Vladimir**, for your advices about research and organizing our nice trip to Serbia. **Yurui**, **Mikael**, and **Kristofer** for your help in the lab practicalities. To the all group members, for fun times in beers tastings, fikas, lunches, dinners, and trips.

All the colleagues from **Biological Physics** and **Physical Chemistry** groups, for creating a nice working environment. **Victoria**, **Deborah**, **Anna**, **Fernando**, **Rafael, Adriana, Carl,** and **Mokhtar** for all nice times and lunches together in sun and indoors, and your friendship.

Mike, **Victoria**, **Anna**, and **Deborah** for taking your time and proofreading my thesis.

Mattias, Pelle, **Marie**, **Daniel, My,** and **Raymond** for making Göteborg more fun.
Mattias, for your support during the writing process.

Irep and **Aldo** for your all encouragement and support, and of course fun times.

Sonya, **Esen**, and **Burcu**, even though we are all in different continents, for being with me all the time.

David, for your love and support.

My family, encouraging me for science since my childhood and for your endless support and love.

References:

[1] J. A Schuller, E.S. Barnard, W. Cai, Y.C. Jun, J.S. White, M.L. Brongersma, Plasmonics for extreme light concentration and manipulation, Nature Materials. 9 (2010) 193–204.

[2] E. Ozbay, Plasmonics: merging photonics and electronics at nanoscale dimensions, Science (New York, N.Y.). 311 (2006) 189–93.

[3] N.J. Halas, Plasmonics: an emerging field fostered by Nano Letters, Nano Letters. 10 (2010) 3816–22.

[4] J. Zhao, L.J. Sherry, G.C. Schatz, R.P. Van Duyne, Molecular Plasmonics: Chromophore–Plasmon Coupling and Single-Particle Nanosensors, IEEE Journal of Selected Topics in Quantum Electronics. 14 (2008) 1418–1429.

[5] A. Csaki, T. Schneider, J. Wirth, N. Jahr, A. Steinbrück, O. Stranik, et al., Molecular plasmonics: light meets molecules at the nanoscale., Philosophical Transactions. Series A, Mathematical, Physical, and Engineering Sciences. 369 (2011) 3483–96.

[6] H. Chen, T. Ming, L. Zhao, F. Wang, L.-D. Sun, J. Wang, et al., Plasmon–molecule interactions, Nano Today. 5 (2010) 494–505.

[7] H. Chen, G.C. Schatz, M. a Ratner, Experimental and theoretical studies of plasmon-molecule interactions., Reports on Progress in Physics. Physical Society (Great Britain). 75 (2012) 096402.

[8] Y.B. Zheng, B. Kiraly, P.S. Weiss, T.J. Huang, Molecular plasmonics for biology and nanomedicine., Nanomedicine (London, England). 7 (2012) 751–70.

[9] H. Fredriksson, Y. Alaverdyan, a. Dmitriev, C. Langhammer, D.S. Sutherland, M. Zäch, et al., Hole–Mask Colloidal Lithography, Advanced Materials. 19 (2007) 4297–4302.

[10] J. Homola, S.S. Yee, G. Gauglitz, Surface plasmon resonance sensors: review, Sensors and Actuators B: Chemical. 54 (1999) 3–15.

[11] S. Nie, S. Emory, Probing Single Molecules and Single Nanoparticles by Surface-Enhanced Raman Scattering, Science. 275 (1997) 1102–1106.

[12] A.J. Haes, C.L. Haynes, A.D. Mcfarland, G.C. Schatz, R.P. Van Duyne, S. Zou, Plasmonic Materials for Surface-Enhanced Sensing and Spectroscopy, MRS Bulletin. 30 (2005) 368–375.

[13] G.L. Liu, Y. Long, Y. Choi, T. Kang, L.P. Lee, Quantized plasmon quenching dips nanospectroscopy via plasmon resonance energy transfer, Nature Methods. 4 (2007) 1015–1017.

[14] Y. Choi, T. Kang, L.P. Lee, Plasmon Resonance Energy Transfer (PRET)-based Molecular Imaging of Cytochrome c in Living Cells, Nano Letters. 9 (2009) 85–90.

[15] H. Atwater, A. Polman, Plasmonics for Improved Photovoltaic devices, Nature Materials. 9 (2010) 205–13.

[16] L. Novotny, S.J. Stranick, Near-filed optical microscopy and spectroscopy with pointed probes, Annual Review of Physical Chemistry. 57 (2006) 303–331.

[17] F. Vollmer, S. Arnold, Whispering-gallery-mode biosensing : label- free detection down to single molecules, Nature Methods. 5 (2008) 591–596.

[18] P. Alivisatos, The use of nanocrystals in biological detection, Nature Biotechnology. 22 (2004) 47–52.

[19] N.R. Guydosh, S.M. Block, Direct observation of the binding state of the kinesin head to the microtubule., Nature. 461 (2009) 125–8.

[20] S.E. Lee, G.L. Liu, F. Kim, L.P. Lee, Remote Optical Switch for Localized and Selective Control of Gene Interference, Nano Letters. 9 (2009) 562–570.

[21] J.R. Lakowicz, Principles of Fluorescence Spectroscopy, 3rd ed., Springer, 2006.

[22] M. Svedendahl, S. Chen, A. Dmitriev, M. Käll, Refractometric sensing using propagating versus localized surface plasmons: a direct comparison., Nano Letters. 9 (2009) 4428–33.

[23] E.C. Le Ru, P.G. Etchegoin, P.D. Diderot, C. Umr, D. Brosse, Mechanisms of Spectral Profile Modification in Surface-Enhanced Fluorescence, The Journal of Physical Chemistry C. 111 (2007) 16076–16079.

[24] B. Sharma, R.R. Frontiera, A. Henry, E. Ringe, R.P. Van Duyne, SERS : Materials , applications , and the future Surface-enhanced Raman spectroscopy (SERS) is a powerful vibrational, 15 (2012) 16–25.

[25] N.T. Fofang, T.-H. Park, O. Neumann, N. a Mirin, P. Nordlander, N.J. Halas, Plexcitonic nanoparticles: plasmon-exciton coupling in nanoshell-J-aggregate complexes., Nano Letters. 8 (2008) 3481–7.

[26] G.L. Liu, Y. Long, Y. Choi, T. Kang, L.P. Lee, Quantized plasmon quenching dips nanospectroscopy via plasmon resonance energy transfer, Nature Methods. 4 (2007) 1015–1017.

[27] K.M. Mayer, J.H. Hafner, Localized surface plasmon resonance sensors, Chemical Reviews. 111 (2011) 3828–57.

[28] S.A. Maier, Plasmonics: Fundamentals and Applications, 2007 editi, Springer, 2007.

[29] C.F. Bohren, D.R. Huffman, Absorption and scattering of light by small particles, Wiley-VCH, 1998.

[30] K. Kneipp, H. Kneipp, I. Itzkan, R.R. Dasari, M.S. Feld, Surface-enhanced Raman scattering and biophysics, Journal of Phys.: Condens. Matter. 14 (2002) R597–R624.

[31] G. McNay, D. Eustace, W.E. Smith, K. Faulds, D. Graham, Surface-enhanced Raman scattering (SERS) and surface-enhanced resonance Raman scattering (SERRS): a review of applications., Applied Spectroscopy. 65 (2011) 825–37.

[32] S. Nie, S. Emory, Probing Single Molecules and Single Nanoparticles by Surface-Enhanced Raman Scattering, Science. 275 (1997) 1102–6.

[33] L. Jensen, C.M. Aikens, G.C. Schatz, Electronic structure methods for studying surface-enhanced Raman scattering., Chemical Society Reviews. 37 (2008) 1061–73.

[34] A. Campion, P. Kambhampati, Surface-enhanced Raman scattering, Chemical Society Reviews. 27 (1982) 241–250.

[35] J.R. Lakowicz, Plasmonics in Biology and Plasmon-Controlled Fluorescence, Plasmonics. 1 (2006) 5–33.

[36] A. Periasamy, R.M. Clegg, FLIM Microscopy in Biology and Medicine, 1 edition, Chapman and Hall/CRC, 2009.

[37] J.I. Gersten, A. Nitzan, Accelerated Energy Transfer Between Molecules Near A Solid Particle, Chemical Physics Letters. 104 (1984) 31–37.

[38] M. Lunz, V. a Gerard, Y.K. Gun'ko, V. Lesnyak, N. Gaponik, A.S. Susha, et al., Surface plasmon enhanced energy transfer between donor and acceptor CdTe nanocrystal quantum dot monolayers., Nano Letters. 11 (2011) 3341–5.

[39] M. Ouyang, H. Huang, N.C. Shaner, A.G. Remacle, S. a Shiryaev, A.Y. Strongin, et al., Simultaneous visualization of protumorigenic Src and MT1-MMP activities with fluorescence resonance energy transfer, Cancer Research. 70 (2010) 2204–12.

[40] E. Kardash, J. Bandemer, E. Raz, Imaging protein activity in live embryos using fluorescence resonance energy transfer biosensors., Nature Protocols. 6 (2011) 1835–46.

[41] N.J. Halas, S. Lal, W.-S. Chang, S. Link, P. Nordlander, Plasmons in strongly coupled metallic nanostructures, Chemical Reviews. 111 (2011) 3913–61.

[42] L. Novotny, Strong coupling, energy splitting, and level crossings: A classical perspective, American Journal of Physics. 78 (2010) 1199.

[43] H. Chen, L. Shao, K.C. Woo, J. Wang, H.-Q. Lin, Plasmonic–Molecular Resonance Coupling: Plasmonic Splitting versus Energy Transfer, The Journal of Physical Chemistry C. 116 (2012) 14088–14095.

[44] X. Wu, S.K. Gray, M. Pelton, Quantum-dot-induced transparency in a nanoscale plasmonic resonator, Optics Express. 18 (2010) 23633–23645.

[45] T. Ambjörnsson, G. Mukhopadhyay, S. Apell, M. Käll, Resonant coupling between localized plasmons and anisotropic molecular coatings in ellipsoidal metal nanoparticles, Physical Review B. 73 (2006) 1–10.

[46] J. Dintinger, S. Klein, F. Bustos, W. Barnes, T. Ebbesen, Strong coupling between surface plasmon-polaritons and organic molecules in subwavelength hole arrays, Physical Review B. 71 (2005) 035424.

[47] J.C. Love, L.A. Estroff, J.K. Kriebel, R.G. Nuzzo, G.M. Whitesides, Self-assembled Monolayers of Thiolates on Metals as a Form of Nanotechnology, Chemical Reviews. 105 (2005) 1103–69.

[48] P.E. Laibinis, G.M. Whitesides, D.L. Allara, Y.-T. Tao, A.N. Parikh, R.G. Nuzzo, Comparison of the Structures and Wetting Properties of Self-Assembled Monolayers of n-Alkanethiols on the Coinage Metal Surfaces, Cu, Ag, Au, Journal of the American Chemical Society. 113 (1991) 7152–7167.

[49] F. Würthner, T.E. Kaiser, C.R. Saha-Möller, J-aggregates: from serendipitous discovery to supramolecular engineering of functional dye materials, Angewandte Chemie (International Ed. in English). 50 (2011) 3376–410.

[50] M. Kasha, H. Rawls, M. El-Bayoumi, The Exciton Model in Molecular Spectroscopy, Pure Appl. Chem. (1965) 371–392.

[51] M. Pope, C. Swenberg, Electronic Processes in Organic Crystals and Polymers, in: Oxford University Press, Oxford, 2nd ed., New York, NY, 1999.

[52] A. Eisfeld, J. Briggs, The J-band of organic dyes: lineshape and coherence length, Chemical Physics. 281 (2002) 61–70.

[53] K. Aslan, V.H. Perez-Luna, Surface Modification of Colloidal Gold by Chemisorption of Alkanethiols in the Presence of a Nonionic Surfactant, Langmuir. 18 (2002) 6059–6065.